

## Computing Multivalued Solutions of Pressureless Gas Dynamics by Deterministic Particle Methods

Alina Chertock<sup>1,\*</sup> and Alexander Kurganov<sup>2</sup>

<sup>1</sup> *Department of Mathematics, NC State University, Raleigh, NC 27695, USA.*

<sup>2</sup> *Mathematics Department, Tulane University, New Orleans, LA 70118, USA.*

Received 14 September 2007; Accepted (in revised version) 6 February 2008

Available online 1 August 2008

---

**Abstract.** We compute multivalued solutions of one- and two-dimensional pressureless gas dynamics equations by deterministic particle methods. Point values of the computed solutions are to be recovered from their singular particle approximations using some smoothing procedure. We study several recovery strategies and demonstrate ability of the particle methods to achieve high resolution.

**AMS subject classifications:** 65M25, 65D10, 65D15, 33F05, 35L67, 35Q60, 76N99

**Key words:** Pressureless gas dynamics equations, semiclassical transport models, deterministic particle methods.

---

### 1 Introduction

We are interested in computing multivalued solutions of the pressureless gas dynamics equations, which, in the two-dimensional (2-D) case, read:

$$\begin{cases} \rho_t + (\rho u)_x + (\rho v)_y = 0, \\ (\rho u)_t + (\rho u^2)_x + (\rho uv)_y = -\rho V_x(x, y), \\ (\rho v)_t + (\rho uv)_x + (\rho v^2)_y = -\rho V_y(x, y), \end{cases} \quad (1.1)$$

where  $\rho$  is the density,  $u$  and  $v$  are the  $x$ - and  $y$ -components of the velocity, respectively, and  $V$  is the potential. These equations arise in the modeling of the formation of large scale structures in the universe [30]. They can be formally obtained as the limit of the isotropic Euler equations of gas dynamics as pressure tends to zero or as the macroscopic limit of a Boltzmann equation when the Maxwellian has zero temperature. The most interesting feature of this model is development of strong singularities — delta-shocks

---

\*Corresponding author. *Email addresses:* [chertock@math.ncsu.edu](mailto:chertock@math.ncsu.edu) (A. Chertock), [kurganov@math.tulane.edu](mailto:kurganov@math.tulane.edu) (A. Kurganov)

both at separate points and along shock surfaces. Because of this, mathematical analysis of pressureless gas dynamics equations is quite complicated. We refer the reader to [2, 4, 5, 13, 28] for some recent results.

Capturing delta-shocks numerically is also a challenging problem. Several finite-volume, kinetic, relaxation methods, as well as methods based on the movement of a system of particles have been proposed in the literature (see, e.g., [1, 3, 10, 22] and references therein). One of them is a sticky particle (SP) method recently developed in [10]. Due to its low dissipation nature, the SP method allows one to accurately capture strong singularities as well as to achieve high resolution of the smooth parts of the solution. The main idea of the SP method was to coalesce approaching particles and to average velocities of the particles located in the same cells of the auxiliary grid. This way a computation of a singular single-valued solution was ensured; see [10] for details.

Pressureless gas dynamics equations also arise in semiclassical approximations of oscillating solutions of the Schrödinger equation with the high frequency initial data (a brief derivation of this model is given in Section 2). In this situation, multivalued solutions—not the (singular) single valued ones—of the pressureless gas dynamics equations are physically relevant (see, e.g., [17]). A number of numerical methods have been recently proposed for computing multivalued solutions in different contexts, see, e.g., [14, 17–21, 23, 27] and references therein.

In this paper, we are interested in capturing multivalued solutions of pressureless gas dynamics using non-dissipative particle methods. We note that none of the aforementioned special SP techniques is needed in the model under consideration. This means that we should allow several particles to be located exactly at the same point (representing several branches of the computed solution!) and to propagate with the velocities that are completely independent of the velocities of their neighbors. The resulting particle method is described in Section 3.

One of the major difficulty in the application of particle methods to the pressureless gas dynamics equations is recovery of the point values of the computed solution from its particle approximation. The commonly used approach—approximation of the Dirac delta functions by its convolution with a smooth kernel (see, e.g., [26])—may not properly work in the case of nonsmooth solutions. Recovery of point values of nonsmooth solutions has been studied in [8], where several possible approaches have been discussed (see also [7, 9]). Recovery of (single valued) solutions from multivalued particle distributions is even more delicate issue since several solution branches have to be averaged. As we demonstrate in Section 4.1, in the one-dimensional (1-D) case, several techniques lead to high resolution nonoscillatory results. The 2-D case is much more complicated, but we are still able to design a satisfactory solution reconstruction, as shown in Section 4.2.

Another difficulty in the application of the deterministic particle method to multivalued solution computations becomes apparent when thin quantum barriers are present, that is, when the potential  $V$  is discontinuous so that the Dirac delta functions appear on the right-hand side (RHS) of (1.1) and (2.3). In this case, we modify the particle method along the lines of [18, 19]: a particle that reaches the barrier may pass it with a certain

probability, depending on the particle velocity and the sign and the size of the jump in the potential. If the probability is between 0 and 1, we split the particle into two particles: one of them transmits through, while the other one reflects from the barrier. The weights of the new particles are proportional to the aforementioned probabilities, and their velocities are computed from the conservation of energy and geometric optics principles. The validity of our approach is supported by both 1-D and 2-D numerical experiments reported in Section 4.

## 2 Description of the model

We consider the Schrödinger equation with the high frequency initial data:

$$\varepsilon\psi_t + \frac{\varepsilon^2}{2}\Delta\psi - V(\mathbf{x})\psi = 0, \quad \psi(\mathbf{x},0) = A_0(\mathbf{x})e^{i(S_0(\mathbf{x})/\varepsilon)}, \quad \mathbf{x} \in \mathbb{R}^n,$$

and use the following multi-phase ansatz:

$$\psi(\mathbf{x},t) = \sum_k A_k(\mathbf{x},t)e^{i(S_k(\mathbf{x},t)/\varepsilon)} + \mathcal{O}(\varepsilon).$$

One may show (see, e.g., [17]) that in the 1-D, the position density,  $m_0^\varepsilon := |\psi|^2$ , the current density,  $m_1^\varepsilon := \varepsilon \operatorname{Im}(\bar{\psi}\psi_x)$ , and the energy density,  $m_2^\varepsilon := -\varepsilon^2(\operatorname{Re}(\bar{\psi}\psi_x) - |\psi_x|^2)/2$ , satisfy the following equations:

$$\partial_t m_0^\varepsilon + \partial_x m_1^\varepsilon = 0, \quad \partial_t m_1^\varepsilon + \partial_x m_2^\varepsilon = -m_0^\varepsilon V'(x).$$

In the single phase case, that is, when

$$\psi(x,t) = A(x,t)e^{i(S(x,t)/\varepsilon)},$$

$m_j^\varepsilon$  do not exhibit oscillations. We then have:

$$m_0^\varepsilon = |A|^2, \quad m_1^\varepsilon = S_x |A|^2, \quad m_2^\varepsilon = (S_x |A|)^2 + \mathcal{O}(\varepsilon^2),$$

and after taking the limit as  $\varepsilon \rightarrow 0$  we obtain the system

$$\partial_t m_0 + \partial_x m_1 = 0, \quad \partial_t m_1 + \partial_x m_2 = -m_0 V'(x), \tag{2.1}$$

which can be closed by using

$$m_2 = \frac{m_1^2}{m_0}. \tag{2.2}$$

Finally, we denote by  $\rho := m_0$  and  $u := m_1/m_0$ , and rewrite the system (2.1)-(2.2) in the form of pressureless gas dynamics equations:

$$\begin{cases} \rho_t + (\rho u)_x = 0, \\ (\rho u)_t + (\rho u^2)_x = -\rho V'(x), \end{cases} \tag{2.3}$$

where  $\rho$  is the density and  $u$  is the velocity.

It is well known (see, e.g., [2,4,5,13,28]) that the system (2.3), as well as its 2-D version (1.1), develop strong singularities (delta-shocks in the density and shocks in the velocity components). However, we are not interested in capturing such solutions. Instead, our goal is to compute multivalued solutions of (1.1) and (2.3). According to the linear superposition principle, the solutions from different branches are to be superimposed. This would result in single valued density and velocities, which are completely different from the aforementioned singular solutions.

**Remark 2.1.** Another convenient tool to derive the semiclassical limit of the Schrödinger equation is the Wigner transform [15,24,29], which gives, in the semiclassical limit, the Liouville (Vlasov) equation in the phase space:

$$f_t + \xi f_x + \eta f_y = V_x f_\xi + V_y f_\eta, \quad (2.4)$$

where  $f = f(x, y, t, \xi, \eta)$  is the density distribution of a physical particle at time  $t$ , position  $(x, y)$ , and traveling with velocity  $(\xi, \eta)$ . The macroscopic quantities (the density and momenta) are then obtained by

$$\rho = \int \int f d\xi d\eta, \quad \rho u = \int \int \xi f d\xi d\eta, \quad \rho v = \int \int \eta f d\xi d\eta.$$

The Liouville equation is also used in the level set method for the computation of multivalued solutions of quasilinear PDEs, [6,20].

### 3 Description of the two-dimensional particle method

We present the 2-D particle method only (its 1-D version can be easily deduced from the 2-D description). We first introduce the vector notation  $\mathbf{w}(\mathbf{x}, t) := (\rho(\mathbf{x}, t), \rho u(\mathbf{x}, t), \rho v(\mathbf{x}, t))^T$ , where  $\mathbf{x} := (x, y)$ , and rewrite the system (1.1) as

$$\mathbf{w}_t + (u\mathbf{w})_x + (v\mathbf{w})_y = -A\mathbf{w}, \quad A(\mathbf{x}) := \begin{pmatrix} 0 & 0 & 0 \\ V_x & 0 & 0 \\ V_y & 0 & 0 \end{pmatrix}. \quad (3.1)$$

We consider (3.1) subject to the initial data

$$\mathbf{w}(\mathbf{x}, 0) = (\rho(\mathbf{x}, 0), \rho u(\mathbf{x}, 0), \rho v(\mathbf{x}, 0))^T, \quad (3.2)$$

and seek the solution of the initial-value problem (3.1)-(3.2) as a linear combination of the Dirac  $\delta$ -functions:

$$\mathbf{w}^N(\mathbf{x}, t) = \sum_{i=1}^N \alpha_i(t) \delta(\mathbf{x} - \mathbf{x}_i(t)) \quad (3.3)$$

with  $\mathbf{x}_i := (x_i, y_i)^T$  and  $\boldsymbol{\alpha}_i := (\alpha_i^{(1)}, \alpha_i^{(2)}, \alpha_i^{(3)})^T$ . Here,  $N$  is a total number of particles,  $\mathbf{x}_i$  is the location of the  $i$ th particle, and  $\alpha_i^{(1)}, \alpha_i^{(2)},$  and  $\alpha_i^{(3)}$  are its mass,  $x$ - and  $y$ -momenta, respectively. The velocities of each particle are then given by  $u_i := \alpha_i^{(2)} / \alpha_i^{(1)}$  and  $v_i := \alpha_i^{(3)} / \alpha_i^{(1)}$ . Substituting (3.3) into the weak formulation of (3.1)-(3.2) results in the following system of ODEs for the locations and the weights of the particles:

$$\begin{cases} \frac{dx_i(t)}{dt} = u_i(t), & \frac{dy_i(t)}{dt} = v_i(t), & \frac{d\alpha_i^{(1)}(t)}{dt} = 0, \\ \frac{d\alpha_i^{(2)}(t)}{dt} = -\alpha_i^{(1)}(t)V_x(\mathbf{x}_i(t)), & \frac{d\alpha_i^{(3)}(t)}{dt} = -\alpha_i^{(1)}(t)V_y(\mathbf{x}_i(t)). \end{cases} \quad (3.4)$$

From here, we obtain  $\alpha_i^{(1)}(t) \equiv \alpha_i^{(1)}(0)$ . Thus, the system (3.4) can be rewritten in a simpler equivalent form:

$$\frac{dx_i(t)}{dt} = u_i(t), \quad \frac{dy_i(t)}{dt} = v_i(t), \quad \frac{du_i(t)}{dt} = -V_x(\mathbf{x}_i(t)), \quad \frac{dv_i(t)}{dt} = -V_y(\mathbf{x}_i(t)), \quad (3.5)$$

which should be solved subject to the initial data

$$\mathbf{x}_i(0) = \mathbf{x}_i^0, \quad u_i(0) = \frac{\rho u(\mathbf{x}_i^0, 0)}{\rho(\mathbf{x}_i^0, 0)}, \quad v_i(0) = \frac{\rho v(\mathbf{x}_i^0, 0)}{\rho(\mathbf{x}_i^0, 0)}.$$

Here,  $\{\mathbf{x}_i^0\}$  are the coordinates of the centers of mass of the nonintersecting domains  $\{\Omega_i\}$  such that the computational domain  $\Omega = \Omega_1 \cup \dots \cup \Omega_N$  and the particles of the masses  $\{\alpha_i^{(1)}(0) := \int \int_{\Omega_i} \rho(\mathbf{x}, 0) d\mathbf{x}\}$  are initially placed at  $\{\mathbf{x}_i^0\}$ .

**Remark 3.1.** The same ODE system (3.5) for the locations of particles and their velocities can be obtained when a deterministic particle method is applied to the Liouville equation (2.4), see [18, 19].

The ODE system (3.5) has to be solved numerically. At the final time, the solution is realized by its particle approximation and its point values have to be recovered. Since in a generic case the particle distribution is irregular, designing a robust point values recovery algorithm is a rather delicate task. In Section 4, we discuss the details of recovery procedures, which, in the case of a smooth potential  $V(\mathbf{x})$ , would complete the construction of the particle method.

There are, however, more complicated situations, in which the potential is discontinuous across a certain curve. Discontinuous potentials model thin quantum barriers that appear in many important physical problems, such as quantum tunneling in semiconductor device modeling, plasmas, and geometrical optics through different materials (see, e.g., [18, 19, 21] and references therein). The mathematical difficulty is related to the fact that the RHS of the system (3.5) consists now of a product of the discontinuous

function and the distribution, which cannot be defined in the sense of distributions. We overcome this difficulty by considering the interaction of the particles with the barrier. In the remaining part of this section, we describe the interaction algorithm, which closely follows the approach from [18, 19].

When a physical particle hits the barrier, it may or may not get through. In general, very fast particles will always pass through the barrier. However, for the intermediate velocities, the situation is uncertain, which means that physical particles may either transmit (with a certain probability  $p_T \in (0, 1)$ ) or get reflected (with the probability  $p_R = 1 - p_T$ ). These probabilities are functions of particle velocities; see [18, 19] and Section 4 for particular examples of such functions. Such an uncertain behavior of the particles may be modeled using a Monte-Carlo approach, but this leads to appearance of stochastic noise that may badly affect the overall resolution of the computed solution. We take advantage of the fact that our particles are *not* the physical ones. So, when the  $i$ th particle interacts with the barrier (we assume that the interaction takes place instantaneously at a certain time moment, say, at  $t = t^*$ ), we simply split the particle into two particles—the reflected ( $i_R$ ) and the transmitted ( $i_T$ ) ones. Right after the interaction, they will be located at the same point, that is,  $\mathbf{x}_{i_R}(t^* + 0) = \mathbf{x}_{i_T}(t^* + 0) = \mathbf{x}_i(t^* - 0)$  and their masses will be proportional to the aforementioned probabilities, that is,

$$\alpha_{i_R}^{(1)}(t^* + 0) = p_{i_R} \alpha_i^{(1)}(t^* - 0), \quad \alpha_{i_T}^{(1)}(t^* + 0) = p_{i_T} \alpha_i^{(1)}(t^* - 0).$$

Finally, the velocities of the new particles will be determined according to the conservation of energy ( $\frac{u^2 + v^2}{2} + V \equiv \text{const}$  across the jump in  $V$ ) and geometric optics principles, see the algorithm below.

We now present a description of the numerical *particle-barrier interaction algorithm*. Let us assume that the particle solution at a certain time  $t = t^c \geq 0$  is available and that no particle will hit the barrier until the  $i$ th particle reaches it at  $t = t^*$  (given the particles configuration at  $t^c$  and the location of the barrier, the next hitting time  $t^*$  can be easily estimated). We then proceed according to Algorithm 3.1.

## 4 Numerical examples

In this section, we present a number of 1-D and 2-D numerical examples to demonstrate the performance of the propose method. In the numerical computations, the ODE system (3.5) has been integrated by the third-order strong stability preserving Runge-Kutta solver, [16]. To initialize the routine, the computational domain was divided into uniform Cartesian cells of size  $\Delta x \times \Delta y$  ( $\Delta x$  in 1-D) and  $N$  particles were placed into the middle of each cell.

As it has been mentioned in Section 3, the crucial component of particle methods is recovery of point values of the (single valued) density and momenta from their multivalued particle distribution (3.3) at the final time. In this paper, we consider and compare three different recovery procedures (listed below as AVE, CONV, and RED). Our results

Algorithm 3.1: Particle-barrier interaction algorithm

- 
1. Numerically solve the system (3.5) on the interval  $(t^c, t^*)$ .
  2. At time  $t = t^*$ , compute the probabilities  $p_{i_R}$  and  $p_{i_T}$  according to the recipes from [18, 19, 21], see also Section 4.
  3. Replace the  $i$ th particle with the  $i_R$ th and the  $i_T$ th ones.
  4. Set  $\alpha_{i_R}^{(1)} = p_{i_R} \alpha_i^{(1)}$  and  $\alpha_{i_T}^{(1)} = p_{i_T} \alpha_i^{(1)}$ .
  5. Compute the velocities of the  $i_R$ th and the  $i_T$ th particles ( $\mathbf{u}_{i_R} := (u_{i_R}, v_{i_R})$  and  $\mathbf{u}_{i_T} := (u_{i_T}, v_{i_T})$ ) from the velocities of the incident particle,  $\mathbf{u}_i := (u_i, v_i)$ , by the following formulae:

$$\mathbf{u}_{i_R} = \mathbf{u}_i - 2(\mathbf{u}_i \cdot \mathbf{n})\mathbf{n}, \quad \mathbf{u}_{i_T} = \mathbf{u}_i + \left( \sqrt{(\mathbf{u}_i \cdot \mathbf{n})^2 - 2[V]} - (\mathbf{u}_i \cdot \mathbf{n}) \right) \mathbf{n}.$$

Here, we assume that the thin barrier is a boundary between two regions,  $R_1$  and  $R_2$ , with the potentials  $V_1(\mathbf{x})$  and  $V_2(\mathbf{x})$ , respectively. The  $i$ th particle propagates from  $R_1$  toward  $R_2$  and hits the barrier at a certain point  $\mathbf{x} = \mathbf{x}^*$ . We denote by  $\mathbf{n}$  the inner unit normal vector for  $R_2$  at  $\mathbf{x}^*$ , and  $[V]$  stands for the jump in  $V$  there, namely,  $[V] := V_1(\mathbf{x}^*) - V_2(\mathbf{x}^*)$ .

6. If two or more particles hit the barrier at time  $t^*$  repeat steps 2-5 for each of them.
  7. Set  $t^c = t^*$  and repeat the entire algorithm until the final computational time is reached.
- 

clearly demonstrate that, in general, none of them can be claimed to be optimal. Designing a robust recovery method is still an open problem.

- **AVE:** The simplest way of regularizing (3.3) is to approximate it by a piecewise constant reconstruction  $\tilde{\mathbf{w}}$  over an auxiliary mesh consisting of nonoverlapping cells  $\{C_j\}_{j=1}^J$  such that  $C_1 \cup \dots \cup C_J = \Omega$  (in our numerical experiments, we have used a uniform Cartesian mesh):

$$\mathbf{w}(\mathbf{x}, t) \approx \tilde{\mathbf{w}}(\mathbf{x}, t) = \frac{1}{|C_j|} \sum_i \alpha_i(t) \chi_{C_j},$$

where  $\chi_{C_j}$  is the characteristic function of the cell  $C_j$ .

- **CONV:** The most widespread way of regularizing (3.3) is to take a convolution product with a with a smooth kernel  $\zeta_\sigma(x)$ :

$$\mathbf{w}(\mathbf{x}, t) \approx (\mathbf{w}^N * \zeta_\sigma)(\mathbf{x}, t) := \sum_{i=1}^N \alpha_i(t) \zeta_\sigma(\mathbf{x} - \mathbf{x}_i(t)),$$

where  $\zeta_\sigma$  serves as a smooth approximation of the  $\delta$ -function which satisfies the following properties:

$$\zeta_\sigma = \frac{1}{\sigma^d} \zeta\left(\frac{\mathbf{x}}{\sigma}\right), \quad \int_{\mathbb{R}^d} \zeta(\mathbf{x}) d\mathbf{x} = 1,$$

where  $\sigma$  is a positive parameter measuring the “width” of the kernel and  $d$  is a number of space dimensions. A wide variety of such kernels and their approximation properties have been extensively discussed in the literature (see, e.g., [11, 12, 26] and references therein). In our numerical experiments, we have used the Gaussian kernel.

• **RED:** The third recovery procedure is based on the particle weights redistribution technique typically used in the immersed boundary method (see, e.g., [25] and references therein). This technique also allows to obtain point values of the redistributed particle approximation at any prescribed set of points. In our numerical experiments, the point values of  $\mathbf{w}$  have been computed at the equally spaced points where the particles were initially placed, namely:

$$\mathbf{w}(x,y,t) \approx \frac{1}{\Delta x \Delta y} \sum_{i=1}^N \alpha_i(t) \phi\left(\frac{|x-x_i(t)|}{\Delta x}\right) \phi\left(\frac{|y-y_i(t)|}{\Delta y}\right),$$

where

$$\phi(r) = \begin{cases} \frac{1}{8} \left(5 - 2r - \sqrt{-7 + 12r - 4r^2}\right), & |r| < 1, \\ \frac{1}{8} \left(3 - 2r - \sqrt{1 + 4r - 4r^2}\right), & 1 < |r| < 2, \\ 0, & \text{otherwise.} \end{cases}$$

**Remark 4.1.** After the point values of  $\mathbf{w} \equiv (\rho, \rho u, \rho v)^T$  have been recovered, the single valued velocities are obtained by  $u = (\rho u) / \rho$  and  $v = (\rho v) / \rho$  (for  $\rho \neq 0$ ).

**Remark 4.2.** In the next section, the solutions reconstructed with the AVE, CONV, and RED procedures will be referred to as the AVE, CONV, and RED solutions.

#### 4.1 One-dimensional examples

**Example 4.1.** We first consider the system (2.3) with  $V(x) = x^2/2$  and subject to the initial conditions

$$\rho(x,0) = 1, \quad u(x,0) = \chi_{(-\infty,0)} - \chi_{(0,\infty)}.$$

This example is taken from [17].

We compute the solution by the particle method with  $N=400$  particles, initially placed on the interval  $[-1,1]$ , and recover it at time  $t=0.2$  using the three different reconstruction procedures outlined above. The obtained results are shown in Figs. 1 and 2. The solid line represents the exact solution obtained in [17]. As one can see, the RED solution (Fig. 1) seems to be the best one: it provides sharp resolution of the discontinuities together with a very high overall accuracy. The CONV solution obtained with  $\sigma = 0.1\sqrt{\Delta x}$  (Fig. 2, right) is also very accurate. However, the CONV procedure is very sensitive to the choice of the regularization parameter  $\sigma$ : when twice smaller  $\sigma$  (Fig. 2, middle) has been taken, the CONV solution becomes oscillatory. The AVE solution (Fig. 2, left) is the least accurate one in this example.

**Example 4.2.** Next, we consider the system (2.3) with zero potential ( $V(x) \equiv 0$ ) and the initial data taken from [17]:

$$\rho(x,0) = 1, \quad u(x,0) = 1\chi_{(-\infty,-0.5)} + (0.3-x)\chi_{(-0.5,0)} + 0.1\chi_{(0,\infty)}.$$

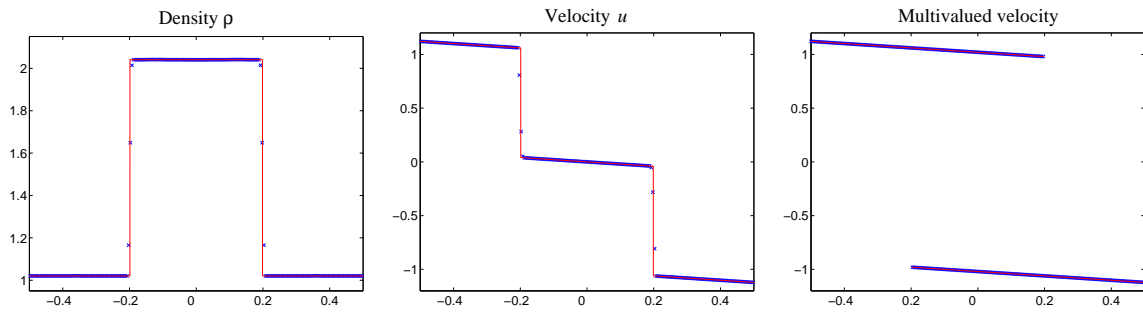


Figure 1: Example 4.1 — the RED solution (left and middle) and the particle velocities (right).

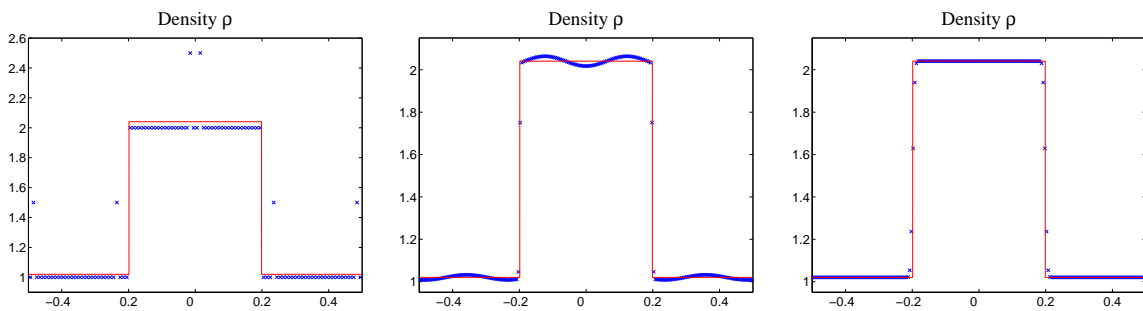


Figure 2: Example 4.1 — the AVE (left) and CONV (with  $\sigma = 0.05\sqrt{\Delta x}$ , middle, and  $\sigma = 0.1\sqrt{\Delta x}$ , right) solutions.

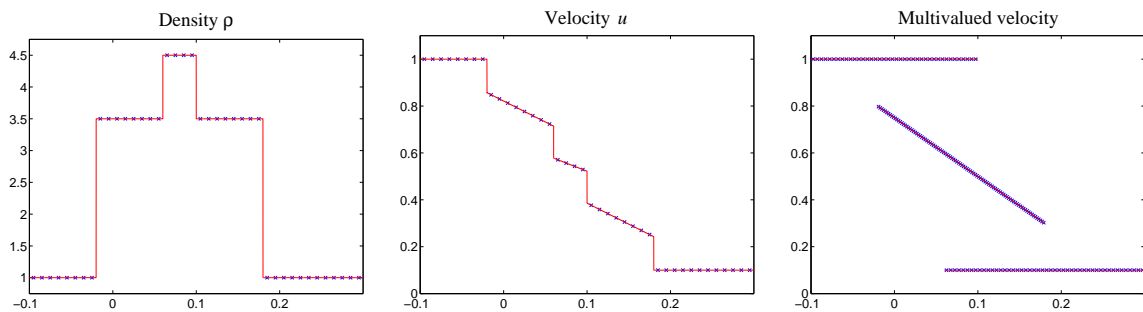


Figure 3: Example 4.2 — the AVE solution (left and middle) and the particle velocities (right).

The solutions computed by the particle method with  $N=400$  particles, initially placed on the interval  $[-1,1]$ , and reconstructed at time  $t = 0.6$  by the three studied recovery procedures are shown in Figs. 3 and 4. Once again, the solid line represents the exact solution, see [17]. One can observe that in this example, all obtained solutions are of a good quality. However, the AVE solution (Fig. 3) is now the best one since all the jumps are perfectly resolved. The CONV solution with  $\sigma = 0.1\sqrt{\Delta x}$  (Fig. 4, right) is the most diffusive one.

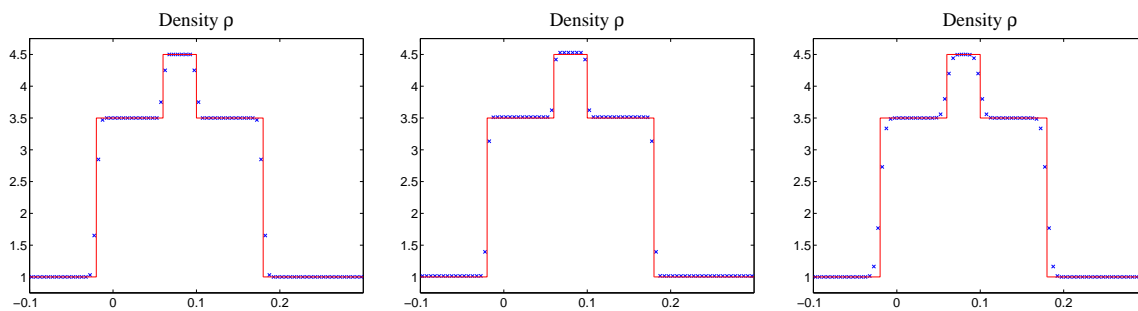


Figure 4: Example 4.2 — the RED (left) and CONV (with  $\sigma = 0.05\sqrt{\Delta x}$ , middle, and  $\sigma = 0.1\sqrt{\Delta x}$ , right) solutions.

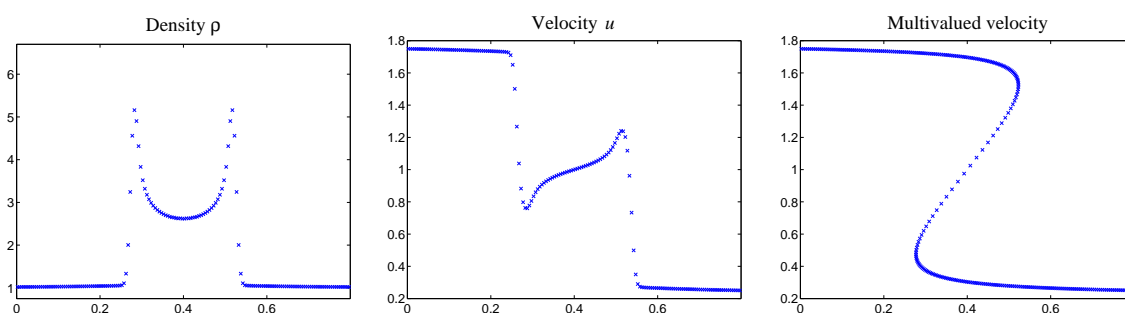


Figure 5: Example 4.3 — the CONV solution with  $\sigma = 0.2\sqrt{\Delta x}$  (left and middle) and the particle velocities (right).

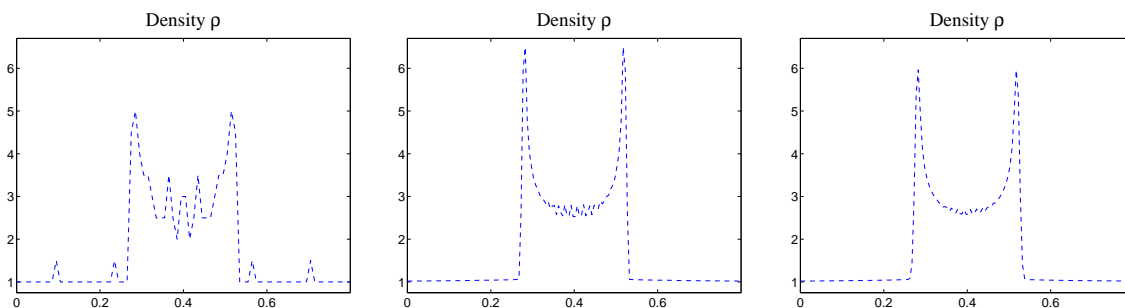


Figure 6: Example 4.3 — the AVE (left), RED (middle), and CONV with  $\sigma = 0.1\sqrt{\Delta x}$  (right) solutions.

**Example 4.3.** In this example (also taken from [17]), the initial conditions for the system (2.3) are given by

$$\rho(x,0) = 1, \quad u(x,0) = 1 - 0.5\arctan(20x),$$

and the potential is  $V(x) \equiv 0$ . An analytical solution of this problem is unavailable.

In Figs. 5 and 6, we plot numerical solutions computed with  $N = 400$  particles, initially placed on the interval  $[-1, 1]$ , and recovered at time  $t = 0.4$ . As one can see in Fig. 6, the

AVE and RED solutions are (very) oscillatory, while the CONV solutions with  $\sigma=0.1\sqrt{\Delta x}$  seems to be of a better quality. When a wider Gaussian is chosen ( $\sigma=0.2\sqrt{\Delta x}$ ), the CONV solution is oscillation-free, but it is more diffusive so that the peaks in the density are much lower, see Fig. 5 (left).

**Example 4.4.** This example is taken from [21]. We consider (2.3) with the initial data  $\rho(x,0)=1$  and

$$u(x,0) = 0.9 \left[ \chi_{(-\infty,-2)} + \left(1 - \frac{(x+2)^2}{4}\right) \chi_{(-2,0)} - \left(1 - \frac{(x-2)^2}{4}\right) \chi_{(0,2)} - \chi_{(2,\infty)} \right],$$

and with the discontinuous potential  $V(x) = 0.2\chi_{(-\infty,0)}$ .

In this case, a particle hitting the barrier will either cross it or be reflected, depending on its incident velocity. The new velocity is then obtained according to the conservation requirement  $\frac{1}{2}u^2 + V \equiv \text{const}$ . Even though there is no uncertainty in the considered setting, the particle-barrier interaction Algorithm 3.1 still applies. There are three possibilities for each particle (see [21]):

- If  $u_i > 0$ , then the  $i$ th particle will cross the barrier ( $p_{i_R} = 0$  and  $p_{i_T} = 1$ ) with the increased velocity  $u_{i_T} = \sqrt{(u_i)^2 + 0.4}$ ;
- If  $u_i < 0$  and  $\frac{1}{2}u_i^2 > 0.2$ , then the kinetic energy is bigger than the potential jump, and the  $i$ th particle will cross the barrier ( $p_{i_R} = 0$  and  $p_{i_T} = 1$ ) with the reduced velocity  $u_{i_T} = -\sqrt{(u_i)^2 - 0.4}$ ;
- If  $u_i < 0$  and  $\frac{1}{2}u_i^2 < 0.2$ , then the kinetic energy is not large enough for the particle to cross the barrier, so the  $i$ th particle will be reflected ( $p_{i_R} = 1$  and  $p_{i_T} = 0$ ) with the positive velocity  $u_{i_R} = -u_i$ .

Notice that in this example, particles do not split and their total number does not change in time.

The solutions computed with  $N=800$  particles, initially placed on the interval  $[-4,4]$ , and reconstructed at time  $t=1.8$  are plotted in Figs. 7 and 8 together with the analytic solution (the solid line), which was calculated in [21]. One can observe that all reconstruction techniques lead to accurate results, though the AVE solution (Fig. 8, left) is more oscillatory than others.

**Example 4.5.** In the last 1-D example (taken from [19]), the discontinuous potential is  $V(x) = 0.5\chi_{(0,\infty)}$  and the initial conditions are given by

$$\rho(x,0) = \sqrt{\frac{100}{\pi}} e^{(-100x+0.5)^2}, \quad u(x,0) = 1 - 0.5(x+0.5).$$

In order to apply the particle method, we utilize a 1-D version of the particle-barrier interaction Algorithm 3.1. To this end, we first compute the probabilities  $p_{i_R}$  ( $p_{i_T}$ ) of the  $i$ th particle to be reflected from (cross) the barrier as suggested in [19]:

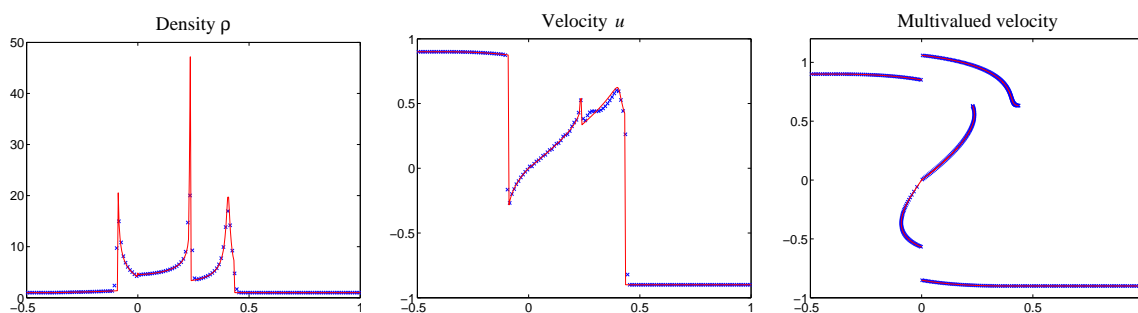


Figure 7: Example 4.4 — the CONV solution with  $\sigma=0.05\sqrt{\Delta x}$  (left and middle) and the particle velocities (right).

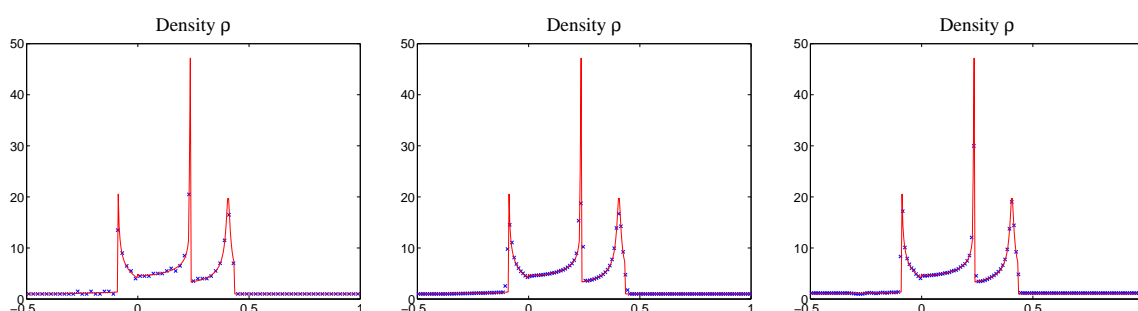


Figure 8: Example 4.4 — the AVE (left), RED (middle), and CONV with  $\sigma=0.1\sqrt{\Delta x}$  (right) solutions.

- If  $u_i < 0$ , then  $p_{i_R} = \left(\sqrt{u_i^2 + 1} + u_i\right)^4$  and  $p_{i_T} = 1 - p_{i_R}$ ;
- If  $0 < u_i < 1$ , then  $p_{i_R} = 1$  and  $p_{i_T} = 0$ ;
- If  $u_i > 1$ , then  $p_{i_R} = \left(\sqrt{u_i^2 - 1} - u_i\right)^4$  and  $p_{i_T} = 1 - p_{i_R}$ .

After the probabilities are computed, we split the particle into two new particles, the reflected ( $i_R$ ) and the transmitted ( $i_T$ ) ones, with the weights proportional to the corresponding probabilities  $p_{i_R}$  and  $p_{i_T}$  and the velocities determined from the conservation requirement as described in Algorithm 3.1.

Initially, we place  $N = 1600$  equally spaced particles in the interval  $[-1, 1]$ . Due to uncertainty in the particle-barrier interactions, the total number of particles increases in time and by the final time  $t = 0.8$  it becomes  $N = 2000$ . In Figs. 9 and 10, we plot the obtained density and multivalued velocity. The RED solution (Fig. 9, left) seems to achieve the sharpest resolution of the density peak, the CONV solution with  $\sigma=0.05\sqrt{\Delta x}$  (Fig. 10) is completely oscillation-free, while the AVE solution is very oscillatory in this example.

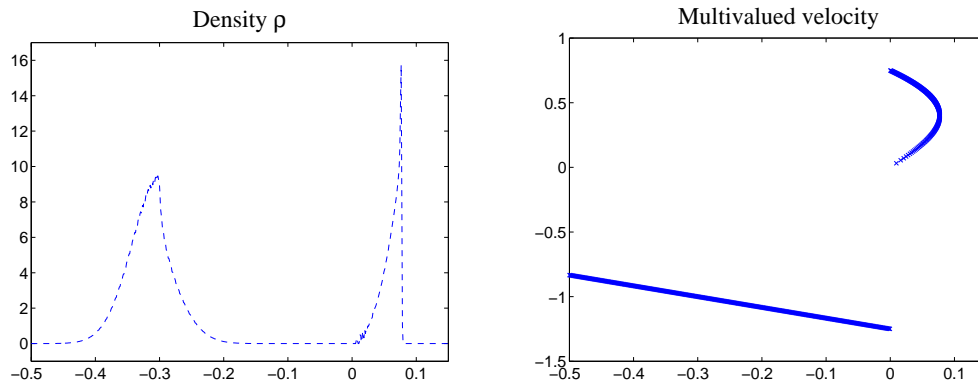


Figure 9: Example 4.5 — the RED solution (left) and the particle velocities (right).

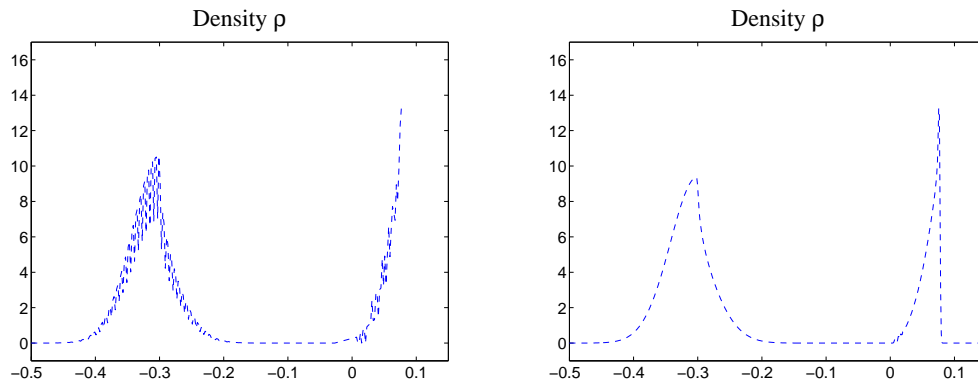


Figure 10: Example 4.5 — the AVE (left) and CONV with  $\sigma = 0.05\sqrt{\Delta x}$  (right) solutions.

### 4.2 A two-dimensional example

Finally, we use the particle method to solve the 2-D system (1.1) with the circular barrier:

$$V(\mathbf{x}) = \begin{cases} 0, & \mathbf{x} \in R_1 := \{\mathbf{x} : |\mathbf{x}| > 1/2\}, \\ 1/2, & \mathbf{x} \in R_2 := \{\mathbf{x} : |\mathbf{x}| < 1/2\}, \end{cases}$$

and subject to the following initial data:

$$\rho(\mathbf{x}, 0) = \frac{8}{\pi} e^{-8(|\mathbf{x}+1|)^2}, \quad \mathbf{u}(\mathbf{x}, 0) \equiv (u(\mathbf{x}, 0), v(\mathbf{x}, 0))^T = (0.75, 0.75)^T.$$

This setting was previously considered in [18]. As in previous two examples, we implement the particle-barrier interaction Algorithm 3.1 and compute the probabilities  $p_{i_R}$  ( $p_{i_T}$ ) of the  $i$ th particle to be reflected from (cross) the barrier. Following [18], we set:

- $p_{i_R} = 1$ , if the  $i$ th particle enters  $R_1$  from  $R_2$  and  $|\mathbf{u}_i| < 1$ ;

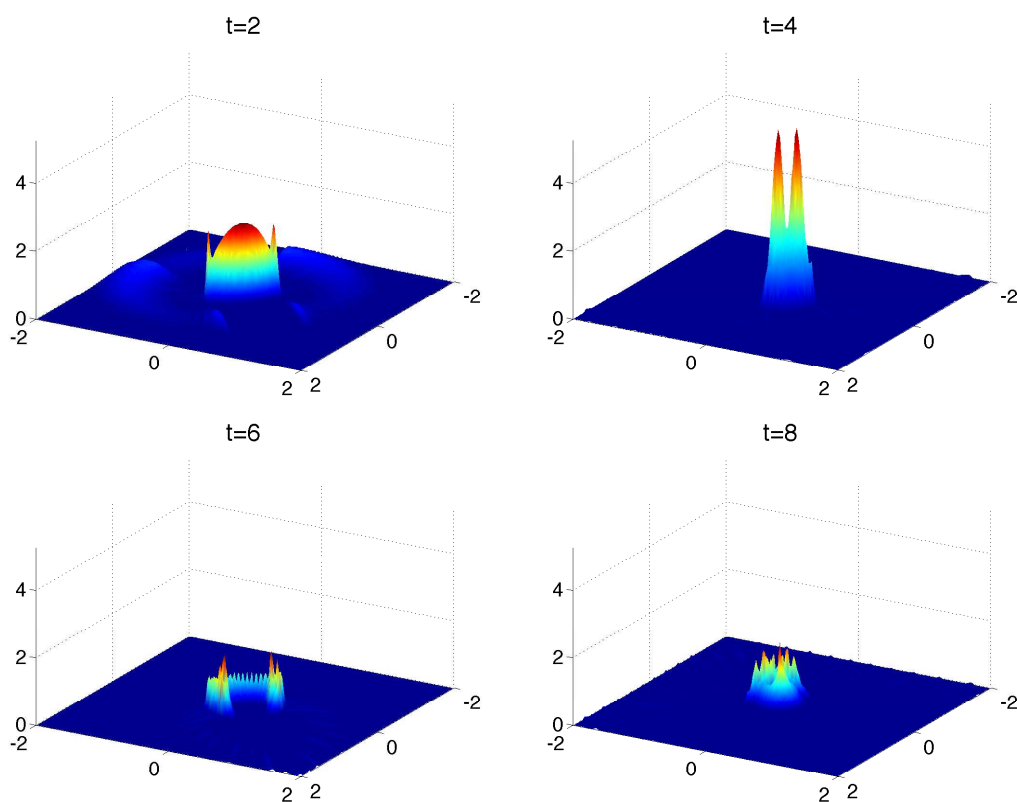


Figure 11: 2-D example — the RED solution (density) computed with  $N=40000$  particles at different times.

- $p_{i_R} = \left| \sqrt{|\mathbf{u}_i|^2 - 1} - |\mathbf{u}_i| \right|^4$ , if the  $i$ th particle enters  $R_1$  from  $R_2$  and  $|\mathbf{u}_i| > 1$ ;
- $p_{i_R} = \left| |\mathbf{u}_i|^2 - \sqrt{|\mathbf{u}_i|^2 + 1} \right|^4$ , if the  $i$ th particle enters  $R_2$  from  $R_1$ .

The probability  $p_{i_T}$  is then obtained as  $p_{i_T} = 1 - p_{i_R}$ . Once both probabilities are computed, we proceed along the lines of Algorithm 3.1.

We now illustrate the performance of the particle method. We start the routine with either  $N=40000$  or  $N=160000$  particles equally spaced over the square domain  $[-2,0] \times [-2,0]$ . In both cases, we recover the solution using the RED procedure at times  $t=2, 4, 6$ , and 8, see Figs. 11 and 12. Since some of the particles that hit the barrier are split into two new particles, the total number of particles increases in time. We note that in this example, which is substantially more complicated than the 1-D examples considered in Section 4.1, the alternative recovery procedures are not robust: the AVE solutions are very oscillatory, while the CONV procedure is extremely sensitive to the selection of the  $\sigma$  parameter.

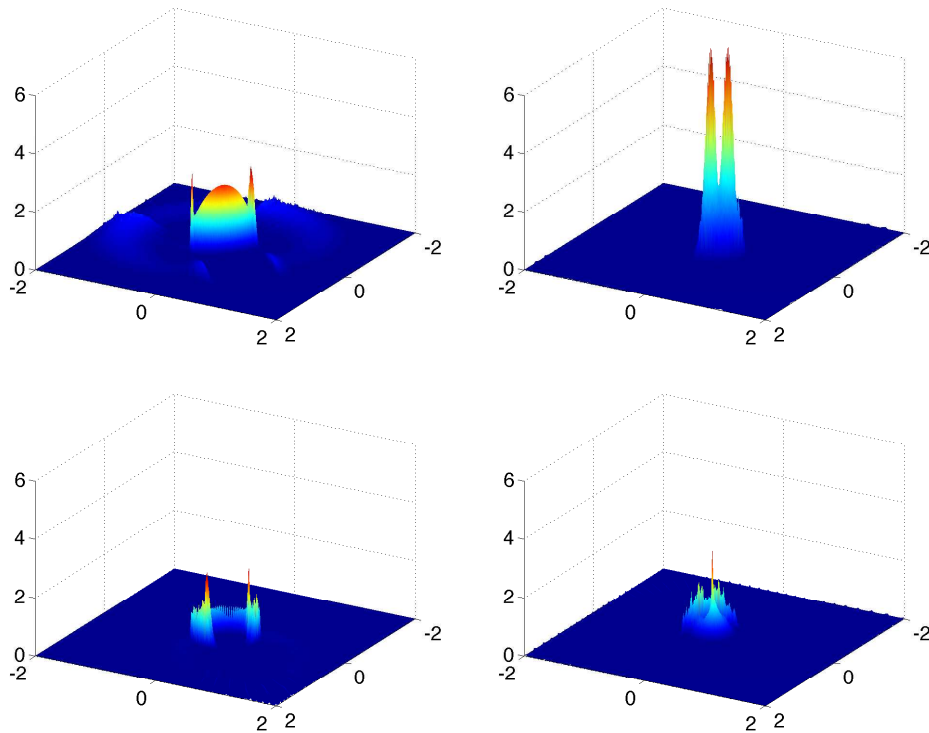


Figure 12: 2-D example — the RED solution (density) computed with  $N=160000$  particles at different times.

## Acknowledgments

We would like to thank Prof. S. Jin for a number of stimulating and encouraging discussions. The research of A. Chertock was supported in part by the NSF Grants DMS-0410023 and DMS-0712898. The research of A. Kurganov was supported in part by the NSF Grant DMS-0610430.

## References

- [1] C. Berthon, M. Breuss, and M.-O. Titeux, A relaxation scheme for pressureless gas dynamics, *Numer. Methods Partial Differential Equations* 22 (2006), 484–505.
- [2] F. Bouchut and F. James, Duality solutions for pressureless gases, monotone scalar conservation laws, and uniqueness, *Comm. Partial Differential Equations* 24 (1999), no. 11-12, 2173–2189.
- [3] F. Bouchut, S. Jin, and X. Li, Numerical approximations of pressureless and isothermal gas dynamics, *SIAM J. Numer. Anal.* 41 (2003), 135–158.
- [4] Y. Brenier and E. Grenier, Sticky particles and scalar conservation laws, *SIAM J. Numer. Anal.* 35 (1998), 2317–2328.

- [5] G.-Q. Chen and H. Liu, Formation of  $\delta$ -shocks and vacuum states in the vanishing pressure limit of solutions to the Euler equations for isentropic fluids, *SIAM J. Math. Anal.* 34 (2003), 925–938.
- [6] L.-T. Cheng, H.-L. Liu, and S. Osher, Computational high-frequency wave propagation using the level set method, with applications to the semi-classical limit of Schrödinger equations, *Commun. Math. Sci.* 1 (2003), no. 3, 593–621.
- [7] A. Chertock and A. Kurganov, On a hybrid finite-volume particle method, *M2AN Math. Model. Numer. Anal.* 38 (2004), 1071–1091.
- [8] A. Chertock and A. Kurganov, On a practical implementation of particle methods, *Appl. Numer. Math.* 56 (2006), 1418–1431.
- [9] A. Chertock, A. Kurganov, and G. Petrova, Finite-volume-particle methods for models of transport of pollutant in shallow water, *J. Sci. Comput.* 27 (2006), 189–199.
- [10] A. Chertock, A. Kurganov, and Yu. Rykov, A new sticky particle method for pressureless gas dynamics, *SIAM J. Numer. Anal.* 45 (2007), 2408–2441.
- [11] A.J. Chorin, Numerical study of slightly viscous flow, *J. Fluid Mech.* 57 (1973), no. 4, 785–796.
- [12] G.-H. Cottet and P.D. Koumoutsakos, *Vortex Methods*, Cambridge University Press, Cambridge, 2000.
- [13] W. E, Yu. G. Rykov, and Ya. G. Sinai, Generalized variational principles, global weak solutions and behavior with random initial data for systems of conservation laws arising in adhesion particle dynamics, *Comm. Math. Phys.* 177 (1996), 349–380.
- [14] B. Engquist and O. Runborg, Computational high frequency wave propagation, *Acta Numer.* 12 (2003), 181–266.
- [15] P. Gérard, P.A. Markowich, N.J. Mauser, and F. Poupaud, Homogenization limits and Wigner transforms, *Comm. Pure Appl. Math.* 50 (1997), no. 4, 323–379.
- [16] S. Gottlieb, C.-W. Shu, and E. Tadmor, High order time discretization methods with the strong stability property, *SIAM Rev.* 43 (2001), 89–112.
- [17] S. Jin and X. Li, Multi-phase computations of the semiclassical limit of the Schrödinger equation and related problems: Whitham vs. Wigner, *Phys. D* 182 (2003), 46–85.
- [18] S. Jin and K.A. Novak, A semiclassical transport model for two-dimensional thin quantum barriers, *J. Comput. Phys.* 226 (2007), 1623–1644.
- [19] S. Jin and K.A. Novak, A semiclassical transport model for thin quantum barriers, *Multiscale Model. Simul.* 5 (2006), 1063–1086.
- [20] S. Jin and S. Osher, A level set method for the computation of multivalued solutions to quasilinear hyperbolic PDEs and Hamilton-Jacobi equations, *Commun. Math. Sci.* 1 (2003), no. 3, 575–591.
- [21] S. Jin and X. Wen, Hamiltonian-preserving schemes for the Liouville equation with discontinuous potentials, *Commun. Math. Sci.* 3 (2005), 285–315.
- [22] R.J. LeVeque, The dynamics of pressureless dust clouds and delta waves, *J. Hyperbolic Differ. Equ.* 1 (2004), 315–327.
- [23] H.L. Liu, S. Osher, and R. Tsai, Multivalued solution and level set methods in computational high frequency wave propagation, *Commun. Comput. Phys.* 1 (2006), no. 5, 765–804.
- [24] G. Papanicolaou and L. Ryzhik, *Waves and transport, Hyperbolic equations and frequency interactions* (Park City, UT, 1995), IAS/Park City Math. Ser., vol. 5, Amer. Math. Soc., Providence, RI, 1999, pp. 305–382.
- [25] C.S. Peskin, The immersed boundary method, *Acta Numer.* 11 (2002), 479–517.
- [26] P.-A. Raviart, An analysis of particle methods, *Numerical methods in fluid dynamics* (Como, 1983), *Lecture Notes in Math.*, vol. 1127, Springer, Berlin, 1985, pp. 243–324.

- [27] O. Runborg, Mathematical models and numerical methods for high frequency waves, Commun. Comput. Phys. 2 (2007), no. 5, 827–880.
- [28] Yu. G. Rykov, On the nonhamiltonian character of shocks in 2-D pressureless gas, Boll. Unione Mat. Ital. Sez. B Artic. Ric. Mat. (8) 5 (2002), 55–78.
- [29] E. Wigner, On the quantum correction for thermodynamic equilibrium, Phys. Rev. 40 (1932), 749–759.
- [30] Ya.B. Zeldovich, Gravitational instability: An approximate theory for large density perturbations, Astron. Astrophys. 5 (1970), 84–89.